



# Sandwich structured PVDF-HFP-based composite solid electrolytes for solid-state lithium metal batteries

Kang Xu<sup>1</sup> · Chao Xu<sup>1</sup> · Yujie Jiang<sup>1</sup> · Jinhai Cai<sup>1</sup> · Jiaxi Ni<sup>1</sup> · Chunyan Lai<sup>1</sup>

Received: 31 March 2022 / Revised: 15 April 2022 / Accepted: 4 May 2022 / Published online: 12 May 2022  
© The Author(s), under exclusive licence to Springer-Verlag GmbH Germany, part of Springer Nature 2022

## Abstract

It is crucial to develop solid electrolyte with good mechanical and electrochemical stability for the application of lithium metal battery. In this work, a sandwich-structured composite solid electrolyte is designed and prepared based on the blend of polyvinylidene fluoride-hexafluoropropylene/polyacrylonitrile (PVDF-HFP/PAN) polymer,  $\text{Li}_{6.46}\text{La}_3\text{Zr}_{1.46}\text{Ta}_{0.54}\text{O}_{12}$  as filler, and a layer of PE film is introduced in the middle to act as a skeleton. The sandwich-structured PVDF-HFP/PAN-10%LLZTO-PE composite solid electrolyte displays a tensile strength of 66.58 MPa, high ionic conductivity of  $2.28 \times 10^{-4}$  S/m at 25 °C, wide electrochemical stable window of 4.8 V, and high lithium ion transfer number of 0.44. The  $\text{LiFePO}_4$  | PVDF-HFP/PAN-10%LLZTO-PE | Li coin battery shows a high specific capacity of 161.9 mAh/g and retains 150.2 mAh/g after 300 cycles at 1 C. Furthermore, the  $\text{LiFePO}_4$  | PVDF-HFP/PAN-10%LLZTO-PE | Li pouch battery shows excellent safety and functionality.

**Keywords** Composite solid electrolyte · Sandwich structure · Lithium dendrite · Solid-state lithium metal battery

## Introduction

Since its commercialization in 1991, lithium-ion batteries (LIBs) have been widely used in portable electronic equipment, electric vehicles, and grid-scale energy storage [1–3]. However, traditional LIBs usually use flammable liquid electrolytes which would easily lead to a variety of safety issues [4, 5]. In addition, the energy density of conventional LIBs using graphite anodes is close to its upper limit, and lithium metal batteries (LMBs) were considered to be the next-generation high-energy density battery [6, 7]. Nevertheless, it is inappropriate to use liquid electrolyte in LMBs, for uneven deposition of Li during operation will result in the formation of lithium dendrites, which will pierce the separator in liquid lithium ion battery and produce short circuits or explosions [8]. An effective solution to the concerns mentioned above is using solid-state electrolytes (SSEs) to replace traditional liquid electrolytes [9]. Compared with liquid electrolytes, SSEs show the advantages of high mechanical strength and

wide electrochemical window and can match the application requirement of lithium metal anode and high voltage cathode, which is essential for enhancing the security and energy density of rechargeable lithium batteries [10, 11]. Xu et al. [12] designed a single-phase and densified PVDF-HFP-based polymer electrolyte with high ionic conductivity and excellent thermal stability, which can be applied in safe LMBs. Wang et al. [13] proposed an ultrathin solid electrolyte with modified polyethylene (PE) as the host and poly(ethylene glycol) methyl ether acrylate and lithium salts as fillers, which has good compatibility, high strength, and safety properties for all solid-state LMBs.

Generally, the SSEs could be classified into inorganic ceramic electrolytes (ICEs), solid polymer electrolytes (SPEs), and composite solid electrolytes (CSEs) [14]. ICEs mainly include NASICON [15], sulfide [16], perovskite lithium lanthanum titanate [17], and garnet  $\text{Li}_7\text{La}_3\text{Zr}_2\text{O}_{12}$  (LLZO) ceramics [18]. Because of its excellent ionic conductivity, negligible electron transport, and outstanding chemical stability, LLZO is regarded as the most promising ICE [19]. Still, ICEs also have some disadvantages, such as poor compatibility with electrodes, poor air stability, and complex synthesis processes, which limit their application [20]. SPEs mainly include plasma electrolytic oxidation (PEO) [21], polyacrylonitrile (PAN) [22], and

✉ Chunyan Lai  
laichunyan@shiep.edu.cn

<sup>1</sup> Shanghai Key Laboratory of Materials Protection and Advanced Materials in Electric Power, Shanghai University of Electric Power, Shanghai 200090, China

poly(vinylidene-co-hexafluoropropylene) (PVDF-HFP) [23]. SPEs have better interface contact properties and simpler preparation process than ICEs; however, the poor ionic conductivity at ambient hampers their development. CSEs composed of polymers and ceramics could not only inherit the advantages of the two groups of components but also overcome their respective shortcomings [24]. With proper composition modulation and appropriate preparation processes, the obtained CSEs may provide the expected properties such as desirable room temperature ionic conductivity, improved electrochemical stable window, enhanced lithium transfer number, and good interface contact [25]. However, the problem of lithium dendrite growth in solid LMB still exists in some cases, resulting in insufficient cycle stability, thus necessitating the design of CSEs that could also suppress Li dendrite growth adequately [26].

In order to improve the mechanical strength and reduce the inter-facial resistance simultaneously, Huo et al. [27] designed a sandwich-type CSE with layered filler. The sandwich-structured CSE was fabricated with a mechanically stable “polymer-in-ceramic” (PIC) inner layer and flexible “ceramic-in-polymer” (CIP) outer layers. The outer layer of the sandwich-type CSE has good wettability, which improves the interface contact between the inner layer and the electrode; the inner layer has good strength and improves the mechanical properties of the composite electrolyte. However, the preparation process of this electrolyte film is complex, for the (PIC) inner layer is very brittle; when it is too thick, it will affect the lithium-ion diffusion; when it is too thin, it cannot bond to the outer layer tightly during the manufacturing.

Herein, a kind of ultra-thin, high-strength sandwich-structured PVDF-HFP/PAN-LLZTO CSEs were designed and synthesized, using  $\text{Li}_{6.46}\text{La}_3\text{Zr}_{1.46}\text{Ta}_{0.54}\text{O}_{12}$  as filler, blended PVDF-HFP and PAN polymers as matrix, and a porous PE film as skeleton in the middle, by solution-casting method. The strong but soft PE film was expected to support the soft PVDF-HFP/PAN/LLZTO mechanically, inhibit the growth of Li dendrites, and prevent cell failure under mechanical deformation. The prepared sandwich-structured CSEs show high ionic conductivity at room temperature, good mechanical properties, wide electrochemical window, good interface stability with lithium anode, and good lithium dendrite inhibition ability.

## Experimental

### Preparation of the $\text{Li}_{6.46}\text{La}_3\text{Zr}_{1.46}\text{Ta}_{0.54}\text{O}_{12}$

$\text{Li}_{6.46}\text{La}_3\text{Zr}_{1.46}\text{Ta}_{0.54}\text{O}_{12}$  was synthesized by solid-state sintering method. In detail,  $\text{Li}_2\text{CO}_3$  (99%+, Damas-Beta),  $\text{La}_2\text{O}_3$  (99.99%, MACKLIN),  $\text{ZrO}_2$  (99%+, Damas-Beta),

and  $\text{Ta}_2\text{O}_5$  (99.99%, Damas-Beta) powders were accurately weighed according to their stoichiometric ratios (excessive 10 wt%  $\text{Li}_2\text{CO}_3$  was used for compensation of lithium losses during sintering). These raw materials were ball milled for 8 h in isopropanol solution at a speed of 400 r/min, and then dried at 80 °C for 14 h. Then, the mixtures were transferred to a magnesium oxide crucible and sintered at 950 °C for 6 h in air atmosphere; some primary powders were obtained. Then, the primary powders were ground in a mortar for 30 min, and transferred to the magnesium oxide crucible, and sintered at 1100 °C for 6 h in air atmosphere. Finally, the LLZTO powder was ball milled again at 400 r/min for 12 h for composite with polymer matrix or subsequent detection.

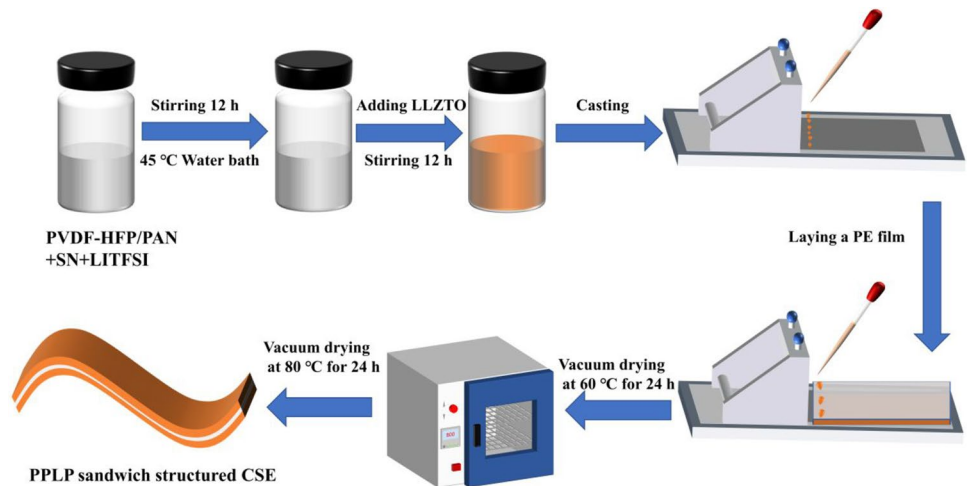
### Preparation of the sandwich-structured composite electrolytes

The sandwich-structured PVDF-HFP/PAN-LLZTO-PE composite electrolyte (abbreviated as PPLP) was fabricated by a solution-casting process as illustrated in Fig. 1. Firstly, 1.8 g PVDF-HFP (Kynar Flex 2801) and 0.2 g PAN ( $M_w = 150\,000$ , MACKLIN) polymers, 0.2 g succinonitrile (SN, 99%+, Damas-Beta), and 0.6 g lithium bis(trifluoromethanesulfonyl)imide (LiTFSI, 99.95%, Sigma-Aldrich) were dissolved in N,N-dimethylformamide (DMF, Damas-Beta), then magnetic stirred at 45 °C for 12 h. Secondly, LLZTO powders were put into the mixture with the LLZTO weight percentage of 0, 5, 10, and 15 wt.% in the total amount of PVDF-HFP, PAN, and LLZTO. The resultant homogenized slurry was then scraped onto both sides of a PE film with a thickness of about 9  $\mu\text{m}$ . Finally, the products were dried at 60 °C for 24 h and then 80 °C for 24 h, and the CSEs with sandwich structure (PPLP0, 5, 10, 15%) were obtained. For comparison, PVDF-HFP/PAN/LiTFSI/SN (PPL0%) and PVDF-HFP/PAN-10%LLZTO/LiTFSI/SN (PPL10%) electrolytes without PE membrane were fabricated on a clean glass sheet and dried according to the same procedure described above. The electrolyte membranes were cut into 19-mm-diameter wafer for the next properties characterization.

### Physical characterization of electrolytes

The crystalline phase of LLZTO powders and the composite electrolytes were investigated by x-ray diffraction (XRD, Rigaku Ultima IV) with  $\text{Cu K}\alpha$  radiation at a scan speed of 5°/min. The particle size distribution of the LLZTO powders was analyzed using a particle size analyzer (Mastersizer 3000). The morphology of LLZTO powders, the surface, and cross-section of the sandwich-structured CSEs were observed by scanning electron microscope (SEM, JEM-7800F). The elemental distribution on the surface of the sandwich-structured CSEs was obtained by

**Fig. 1** Schematic presentation of the sandwich structured PVDF-HFP/PAN-LLZTO-PE CSE preparation process



energy-dispersive X-ray spectroscopy (EDS). The tensile strength of PPL CSEs and PPLP sandwich-structured CSEs was tested by a universal testing machine (WDW-5). The thermal properties of the pure PVDF-HFP powders, LLZTO powders, PPLP0%, and PPLP10% composite electrolytes were investigated through TGA (STA449C/3/G) at 10 °C min<sup>-1</sup> in air atmosphere from room temperature to 600 °C.

### Electrochemical characterization of electrolytes

Electrochemical impedance spectroscopy (EIS) of symmetrical stainless steel was tested on the electrochemical station (CHI660E) with a frequency range of 10<sup>6</sup>–10<sup>-2</sup> Hz and an alternating current (AC) amplitude of 10 mV to study the temperature dependence of the ionic conductivity of the sandwich-structured CSEs (25–90 °C). The ionic conductivity ( $\sigma$ ) was calculated according to Formula (1):

$$\sigma = \frac{L}{RS} \tag{1}$$

where  $L$  (cm) is the thickness of the sandwich-structured PPLP CSEs,  $R$  ( $\Omega$ ) is the total resistance of the sandwich-structured PPLP CSEs, and  $S$  (cm<sup>2</sup>) is the area of stainless steel electrode. The electrochemical stability of the sandwich-structured PPLP CSEs was characterized by linear sweep voltammetry (LSV) of the Li | PPLP | SS battery at a scan rate of 0.5 mV/s and 25 °C in 2.5–5.5 V. The transfer number of lithium ion ( $t_{Li^+}$ ) was tested in symmetrical Li | PPLP | Li battery by the AC impedance DC polarization method and can be calculated by Formula (2):

$$t_{Li^+} = \frac{I_{SS}(\Delta V - I_0 R_0)}{I_0(\Delta V - I_{SS} R_{SS})} \tag{2}$$

where  $\Delta V$  is the applied DC voltage (10 mV) and  $I_0$  and  $I_{SS}$  are the initial current and steady-state current in the DC

polarization process, respectively.  $R_0$  and  $R_{SS}$  are the initial and steady-state charge transfer resistance in the DC polarization process, respectively.

### Characterization of coin battery

To evaluate the electrochemical properties of electrolytes, LiFePO<sub>4</sub> | electrolyte | Li and Li<sub>4</sub>Ti<sub>5</sub>O<sub>12</sub> | electrolyte | Li coin batteries were assembled. The cathode active materials consists of LiFePO<sub>4</sub> or Li<sub>4</sub>Ti<sub>5</sub>O<sub>12</sub>, carbon black, and PVDF in an 8:1:1 weight ratio. The active material load of the cathode electrode (LiFePO<sub>4</sub> or Li<sub>4</sub>Ti<sub>5</sub>O<sub>12</sub> type) was around 1.2–1.5 mg/cm<sup>2</sup>. In order to further improve the interface contact, little fluoroethylene carbonate (~ 2  $\mu$ L/cm<sup>2</sup>) was added between the cathode and the electrolyte membrane before the battery was assembled. The CV test of the LiFePO<sub>4</sub> | electrolyte | Li battery was conducted in 2.5–4.2V at a scanning speed of 0.1 mV/s.

### Characterization of pouch battery

To verify the practical applicability of the sandwich-structured CSE, pouch batteries with LiFePO<sub>4</sub> cathode (length 5 cm, width 4 cm, loading 9.5–10.5 mg/cm<sup>2</sup>), the sandwich-structured PPLP10% CSE membrane (length 5.4 cm, width 4.5 cm) and a Li foil (length 5.2 cm, width 4.2 cm) were assembled in an argon-filled glove box (O<sub>2</sub><0.01 ppm, H<sub>2</sub>O<0.01 ppm) and measured by a LAND-CT2001A system.

### Results and discussion

As illustrated in Fig. 2a, the XRD pattern of as-prepared LLZTO agrees well with the standard PDF card (JCPDS#80-0457), indicating that the synthesized LLZTO has pure

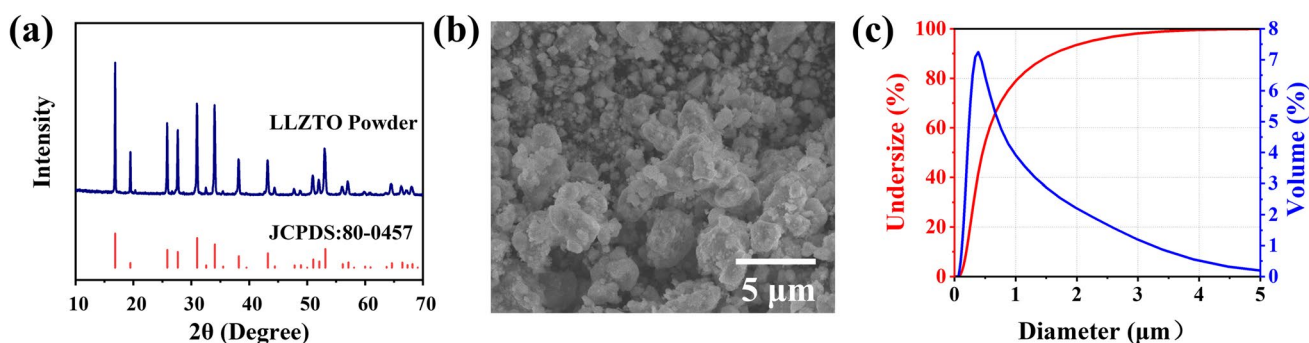


**Fig. 2** **a** XRD patterns of the as-prepared  $\text{Li}_{6.46}\text{La}_3\text{Zr}_{1.46}\text{Ta}_{0.54}\text{O}_{12}$  powder and the standard cubic  $\text{Li}_7\text{La}_3\text{Zr}_2\text{O}_{12}$  (PDF#80-0457), **b** the SEM image, and **c** the particle size and distribution of as-prepared  $\text{Li}_{6.46}\text{La}_3\text{Zr}_{1.46}\text{Ta}_{0.54}\text{O}_{12}$

cubic crystal structure, and Ta element has been successfully doped into the lattice of LLZO [28]. The Ta doping will reduce the lattice parameter of LLZO and make it have stronger atomic bonds, which will improve the mechanical properties of LLZO. As well known, cubic was the expected phase because the LLZO with this crystal form usually has high ionic conductivity reaching to  $1.0 \times 10^{-3}$  S/cm, high lithium ion transfer number near to 1, and chemical stability to lithium metal [29]. In addition to the effect of microstructure, grain size also affects the mechanical properties of LLZO ICE. Smaller particle size of LLZO can improve the grain boundary contact area of the electrolyte, and the internal stress can be dispersed more evenly, thereby inhibiting

the growth of lithium dendrites. The SEM images in Fig. 2b shows that LLZTO ceramic are small powders with diameters ranging from 0.1 to 5.0  $\mu\text{m}$ . As can be seen from Fig. 2c, the  $D_{10}$ ,  $D_{50}$  (average particle size), and  $D_{90}$  diameters of LLZTO powders are 192 nm, 458 nm, and 1.624  $\mu\text{m}$ , respectively. The average particle size of LLZTO powders reaches sub-micron level, which could meet the size requirement of composite with polymer matrix.

Figure 3 displays the SEM photos of the PPLP0% SPE membrane; PPLP10% CSE membrane; EDS mapping of F, La, Zr, and Ta in the PPLP10% membrane; PE film; and the cross-section of PPLP10% CSE. As shown in Fig. 3a, the surface of the PPLP0% membrane is relatively rough with

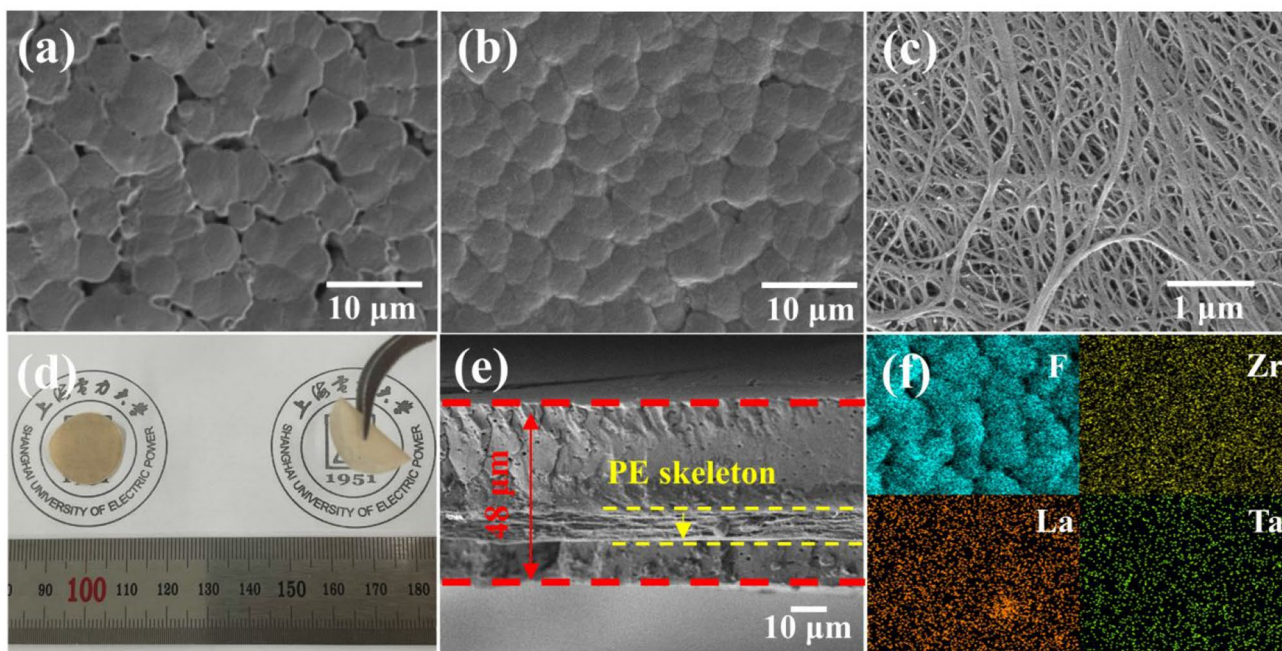


**Fig. 3** **a**, **b** The SEM image of sandwich-structured PPLP0% and PPLP10% membrane, **(c)** the SEM image of PE film, **(d)** flexibility demonstration of a bendable sandwich-structured PPLP10% mem-

brane, **(e)** the SEM image of sandwich-structured PPLP10% CSE cross-section, **(f)** EDS mapping of F, Zr, La, and Ta in PPLP10% CSE

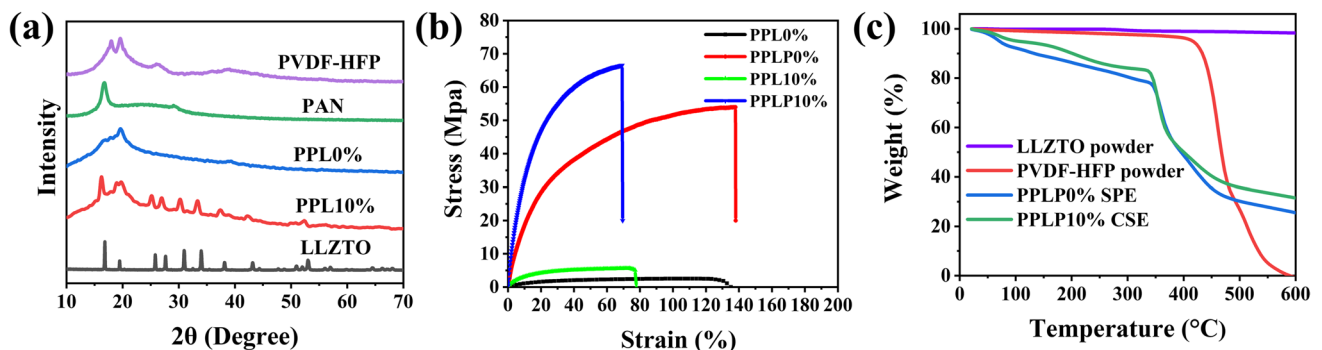
some discontinuous holes, which has a negative impact on the conduction of lithium ions. It could be observed from Fig. 3b that after the addition of LLZTO filler, the surface of the PPLP10% sandwich-structured CSE membrane becomes smooth and dense, which is beneficial to the ionic conductivity and mechanical strength of PPLP10%. This phenomenon can be explained by the strong Lewis acid-base interactions between the LLZTO filler and the segmental chains of the blended polymer, which also indicates that LLZTO is uniformly distributed in the PVDF-HFP/PAN matrix [30]. As presented in Fig. 3c, the PE film has a continuous porous structure, which ensures the full penetration of slurry without strength losing. Furthermore, the PE film is very thin (about 9 μm), which can enhance the mechanical strength of sandwich-structured CSEs without energy density reducing of solid-state batteries. As shown in Fig. 3d, for testing the flexibility of sandwich-structured PE-reinforced composite electrolyte film, a bending experiment was conducted. PPLP10% CSE films could be bent with tweezers without separation and cracking and can be restored as before, indicating that it has good flexibility and excellent processing properties. Figure 3e is a cross-sectional view of the PPLP10% CSE membrane, from which an obvious sandwich structure could be seen clearly; the PE skeleton located in the middle of the two electrolyte layers can support the CSEs on both sides effectively. Figure 3f exhibits the EDS mapping of F, Zr, La, and Ta elements in PPLP10% CSE membrane, indicating that the LLZTO filler is uniformly distributed in the blended polymer without significant agglomeration. The uniform distribution of the filler in CSEs is critical to the improvement of electrochemical properties and thermal properties of sandwich-structured PPLP CSEs.

Figure 4a shows the XRD patterns of LLZTO powder, PPL10% CSE membrane, PPL0% SPE membrane, pure PAN SPE, and pure PVDF-HFP SPE. The results demonstrate that PVDF-HFP is not completely crystallized, with three diffraction peaks approximately at 17.9°, 20.0°, and 27.0°, referring to the crystal planes (100), (020), and (110),

respectively [31]. The XRD pattern of PPL0% displays a broad peak at 17.97°, the crystalline peak of pure PAN at 16.8°, the crystalline peak at 18.2° and 26.6° of PVDF-HFP all disappeared. It can be explained by the physical interaction between SN and the blended polymer. The incorporation of LLZTO decreased the crystallization peak intensity of the blend polymer, which was attributed to the fact that LLZTO powders changed the polymer chain segments into a disordered state. The XRD pattern of LLZTO in PPL10% CSE membrane exhibits no evident change compared to the pure LLZTO powder, showing that LLZTO powders could exist stably in the PVDF-HFP/PAN matrix.

The mechanical properties of solid-state electrolytes affect the structure integrity of cathode and anode electrodes significantly, and the mechanical stability of solid-state LMBs is heavily reliant on solid-state electrolyte [32]. When the stress inside the solid-state LMBs exceeds the strength of the electrolyte, different types of mechanical failure will occur in the battery, which seriously deteriorates the electrochemical performance of solid-state LMBs. As shown in Fig. 4b, compared with PPL0% SPE membrane, the tensile strength of PPL10% CSE membrane with LLZTO increased from 2.54 MPa to 5.63 MPa, the improvement effect was not obvious. In contrast, after the introduction of PE film, the tensile strength of PPLP0% SPE membrane and PPLP10% CSE membrane was improved obviously and reached 53.94 MPa and 66.58 MPa, respectively. The perfect mechanical strength of the sandwich-structured solid electrolyte could ensure the long-time operation of solid-state LMBs without mechanical failure and make it safer [33].

The thermal performance of the electrolyte is an important factor in the safety of solid-state LMBs. Figure 4c shows the comparative thermal-gravimetric analysis (TGA) traces of LLZTO powder, PVDF-HFP powder, PPLP0% SPE membrane, and PPLP10% CSE membrane. As presented in the TGA curves, the prepared LLZTO ICE has little mass loss before 250 °C, but a little mass loss between 250 °C and 600 °C, which might be the removal of the trapped



**Fig. 4** a XRD patterns of LLZTO powder, PPL10% CSE membrane, PPL0% SPE membrane, the pure PAN SPE, and pure PVDF-HFP SPE, b stress-strain curves of PPL0%, PPL10%, PPLP0%, and

PPLP10% membrane, c TGA curves of the LLZTO and PVDF-HFP powder, PPLP0%, and PPLP10% membrane

moisture. Overall, the thermodynamic property of LLZTO powders is very stable, which is significant for the safety performance of the PPLP10%. The pure PVDF-HFP powder is thermally stable before 450 °C, and there is significant weight loss after 450 °C. For PPLP0% SPE membrane and PPLP10% CSE membrane, the weight loss until 340 °C is related to the thermal decomposition of the PAN, and the degradation of SN, partial lithium salts, and water absorbed in the air [34]. In addition, for PPLP10% CSE membrane, the increase of amorphous part caused by the interaction of LLZTO, LiTFSI, and polymer matrix also reduces the thermal decomposition temperature. In a sense, the thermodynamic property of the sandwich-structured PPLP10% CSE membrane could meet the application requirements of most solid-state LMBs.

Figure 5a displays the ionic conductivity variation of sandwich-structured PPLP CSEs containing 0 wt%, 5 wt%, 10 wt%, and 15 wt% LLZTO at different temperatures (25–90 °C). When the content of LLZTO is in the range of

0–10 wt%, with the increase of LLZTO content, the ionic conductivity of sandwich-structured PPLP CSEs increases significantly; this is mainly due to the improved segment mobility of PVDF/PAN matrix and the excellent  $\text{Li}^+$  conductivity of LLZTO. The synergistic effect of the two aspects leads to the increase of ionic conductivity of sandwich structured PPLP CSE membrane, and the sandwich-structured PPLP10% CSE shows the highest value of  $2.28 \times 10^{-4}$  S/cm at 25 °C. However, when the content of LLZTO exceeds 10 wt%, the ionic conductivity of sandwich-structured PPLP CSE decreased, which may be due to the introduction of holes in the composite electrolyte by excessive LLZTO powders, and the discontinuous structure hindered the conductivity of  $\text{Li}^+$  [35]. With the increase of temperature, the ionic conductivity of four sandwich-structured PPLP CSEs increases, and the Arrhenius curves (25–90 °C) of solid electrolytes were obtained as illustrated in Fig. 5b. By observing the slope of the Arrhenius curves of the sandwich-structured PPLP CSEs, it is clearly seen that the activation energy ( $E_a$ )

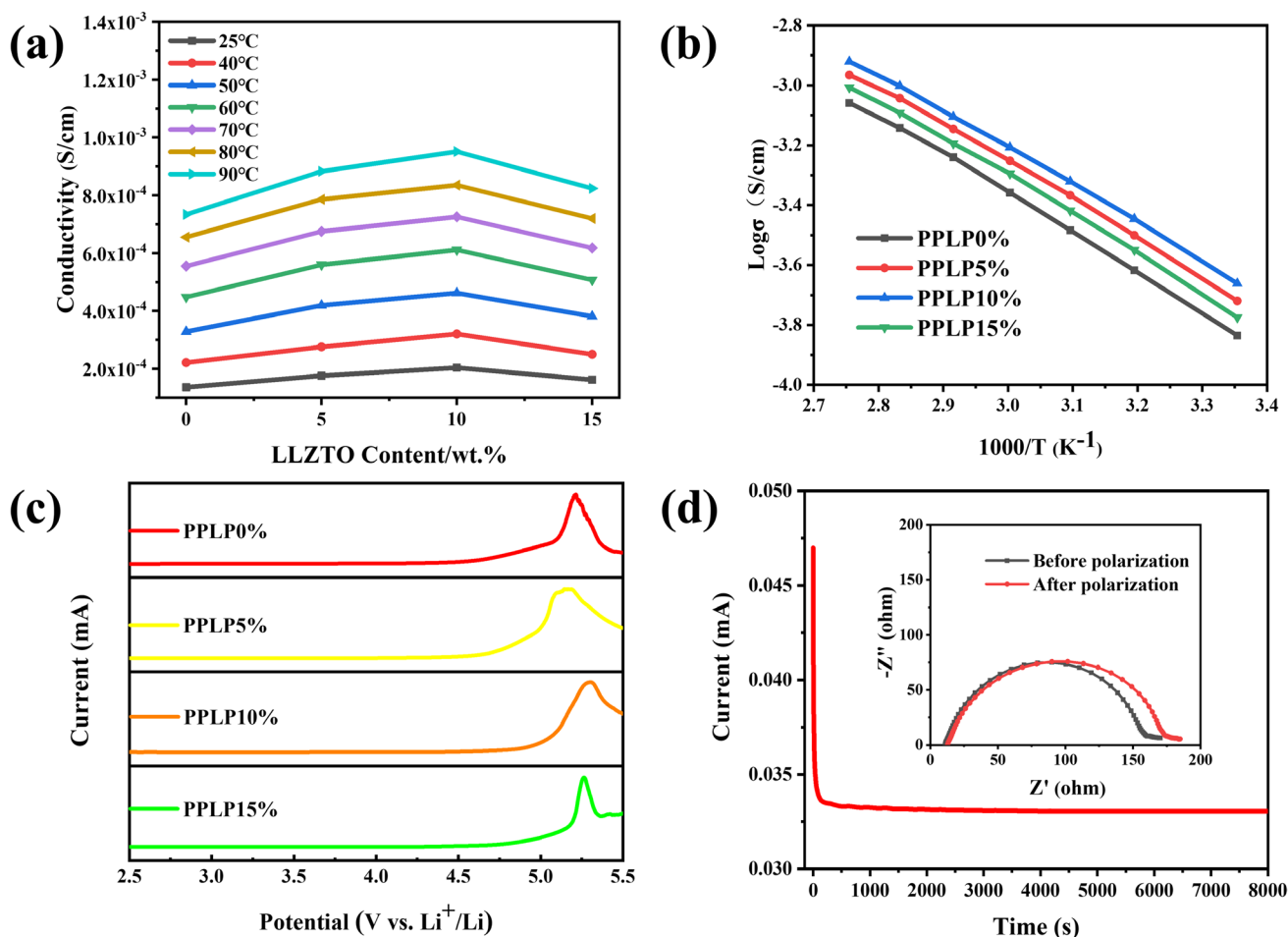


**Fig. 5** a Ion conductivity of sandwich-structured PVDF-HFP/PAN-x%LLZTO-PE CSEs ( $x = 0, 5, 10, 15$ ) at different temperature. b Arrhenius plots of sandwich-structured PVDF-HFP/PAN-x%LLZTO-PE CSEs ( $x = 0, 5, 10, 15$ ), c LSV curves of sandwich-structured

PVDF-HFP/PAN-x%LLZTO-PE CSEs ( $x = 0, 5, 10, 15$ ), d current-time curve at a polarization voltage of 10 mV of sandwich-structured PPLP10% CSE membrane; the inset is EIS diagram before and after the polarization

of the PPLP10% CSE is the smallest, and the smaller  $E_a$  indicates the easier process of lithium ion migration.

The LSV curves of the prepared sandwich-structured PPLP CSEs with four different LLZTO contents are shown in Fig. 5c. It can be clearly seen that the electrochemical window of PPLP0% SPE membrane is about 4.4 V. Meanwhile, with the increase of LLZTO content, the electrochemical window of sandwich-structured PPLP CSEs is also improved (0–10 wt%), which is due to the excellent electrochemical window of LLZTO. However, when the content of LLZTO exceeded 10 wt%, the electrochemical window decreased, which may be related to the discontinuous aggregation distribution of excess LLZTO in the electrolyte membrane. In this work, the sandwich-structured PPLP10% CSE membrane shows a widest electrochemical window of 4.8 V, which can meet the requirements of high-voltage cathode material and improve the energy density of solid LMBs.

The lithium ion transfer number of solid electrolytes shows a significant effect on the polarization of the battery during charging and discharging. As shown in Fig. 5d, the lithium ion transfer number of the sandwich-structured PPLP10% CSE membrane calculated by Formula (2) was 0.44, higher than that of conventional liquid electrolyte mainly ranging from approximately 0.2 to 0.4. The reason for the high lithium ion transfer number of sandwich-structured PPLP10% CSE is that the addition of SN promotes the decomposition of LITFSI and increases the concentration of TFSI<sup>-</sup>, so that a larger proportion of lithium ion can be transported [36]. Moreover, the lithium ion transfer number of LLZTO is close to 1, which provides a large number of active sites to react with lithium salts [37]. In addition, a large number of lithium ion in the system can react with the  $-C\equiv N$  groups in PAN, which also contributes to the increase of the lithium ion transfer number in the sandwich-structured PPLP10% CSE [30, 38].

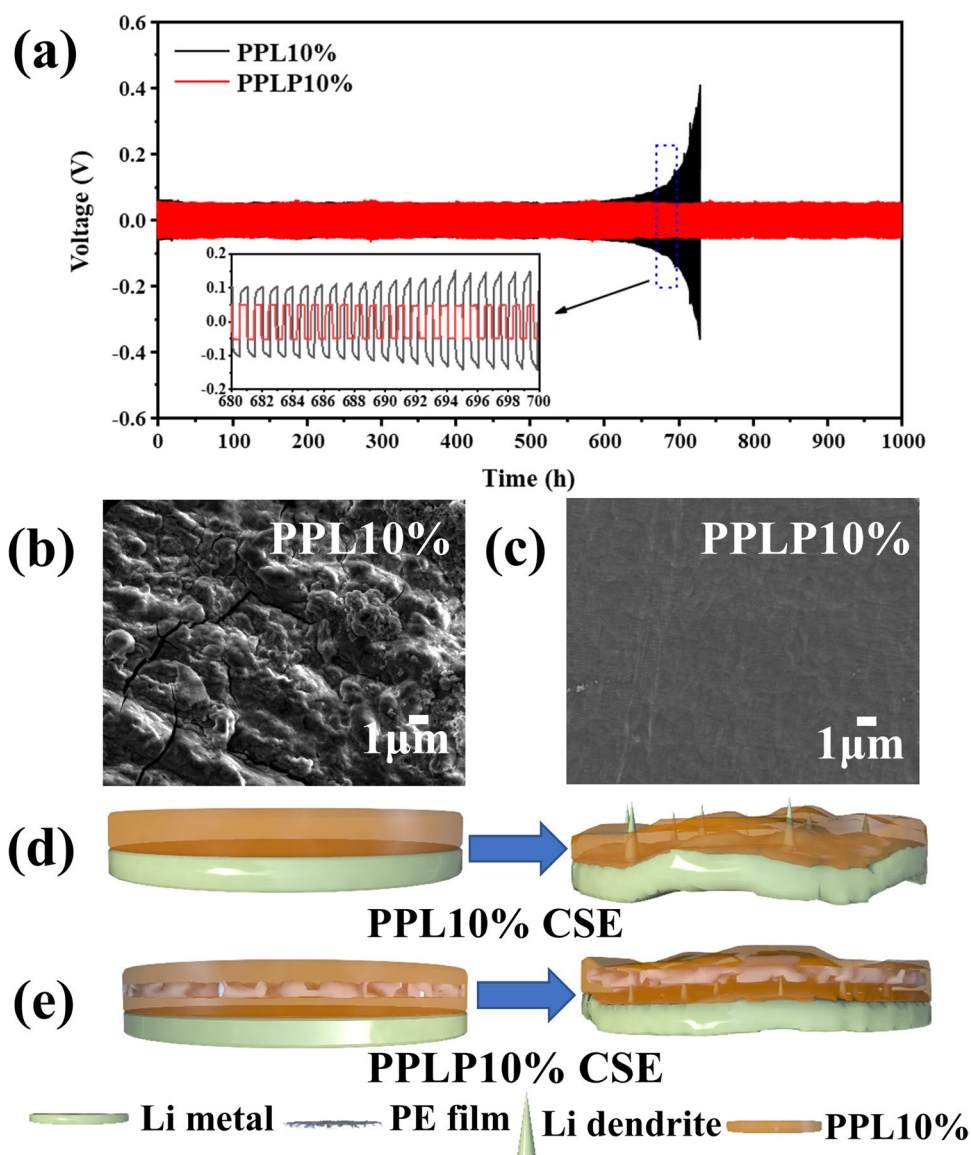
In order to test the cycling stability of CSEs during the Li plating and stripping processes, Li symmetric batteries with PPL10% and PPLP10% were assembled. It can be seen from Fig. 6a that the internal short circuit of Li | PPL10% | Li symmetric battery occurred after 700 h at a current density of 0.10 mA/cm<sup>2</sup>. In contrast, the symmetrical lithium battery Li | PPLP10% | Li with a sandwich-structured solid electrolyte film could cycle stably for about 1000 h without failure. As shown in Fig. 6b, after 700 h cycling in Li | PPL10% | Li symmetric cell, the Li metal surface presents a porous rough structure, which may be due to the growth of lithium dendrites. On the contrary, the surface of Li metal in Li | PPLP10% | Li symmetric battery is still smooth even after 1000 h cycle, and no dendrite structure is detected, as illustrated in Fig. 6c, indicating that the sandwich-structured PPLP10% CSE membrane has better mechanical and electrochemical stability with lithium metal, which could inhibit the growth of lithium dendrite. The mechanism of the above

phenomenon can be explained by Fig. 6d, e. It can be seen from Fig. 6d that before the cycle of Li | PPL10% | Li symmetric battery, PPL10% is a smooth and dense solid-state electrolyte membrane. During the long cycle, the PPL10% CSE without PE film gradually changes to a viscous gel state because of its poor mechanical strength, which easily causes the PPL10% CSE to be pierced by lithium dendrites, and the Li | PPL10% | Li symmetric cell fails as a result. As shown in Fig. 6e, in contrast, the sandwich-structured PPLP10% CSE promotes the uniform deposition of lithium ion on the lithium metal surface and inhibits the growth of lithium dendrites effectively. In addition, the PE film in the middle of the sandwich-structured PPLP10% CSE membrane provides a solid framework for PPLP10%, which greatly improves the mechanical properties to resist the piercing effect of lithium dendrites.

Based on the above results, LiFePO<sub>4</sub> | PPLP10% | Li battery was assembled. Figure S1 displays the CV curves of LiFePO<sub>4</sub> | PPLP10% | Li cell for the initial three cycles at a scan speed of 0.1 mV/S over a potential range of 2.5–4.2 V (vs. Li/Li<sup>+</sup>). There are two characteristic peaks of LiFePO<sub>4</sub>, corresponding to the reduction reaction at 3.2 V and oxidation reaction at 3.65 V, respectively. No other peaks are found during the cycle, indicating that no obvious side reaction occurred. From the highly similar three CV curves, it can be speculated that the battery with PPLP10% CSE membrane has high electrochemical stability and reversible behavior.

The rate performance of LiFePO<sub>4</sub> | PPL10% | Li and LiFePO<sub>4</sub> | PPLP10% | Li solid-state LMBs at room temperature is exhibited in Fig. 7a. It can be seen that from 0.1 C to 2 C, and then to 0.1 C, both batteries can recover their original capacity. LiFePO<sub>4</sub> | PPLP10% | Li battery shows better rate performance due to its perfect electrochemical properties and excellent mechanical properties. At the current densities of 0.1 C, 0.5 C and 1 C, the specific discharge capacities of LiFePO<sub>4</sub> | PPL10% | Li battery were 171.2 mAh/g, 167.2 mAh/g, and 160.5 mAh/g, respectively, with little attenuation. However, when the current density reached 2 C, the specific discharge capacity of LiFePO<sub>4</sub> | PPL10% | Li battery decreased relatively fast, to 143.2 mAh/g, but it was still significantly better than that of LiFePO<sub>4</sub> | PPL10% | Li battery (about 112.2 mAh/g). This shows that the rate performance of solid-state LMBs can be significantly improved by using the sandwich-structured solid electrolyte, which is important for the rapid charge and discharge performances of the battery. Figure 7b is the charging and discharging curves of the LiFePO<sub>4</sub> | PPLP10% | Li solid-state battery at room temperature with different rates in 2.5–4.2 V. It can be obviously seen that the polarization of LiFePO<sub>4</sub> | PPLP10% | Li battery is very small at low charge and discharge rates ( $\leq 1$  C). The low polarization of the LiFePO<sub>4</sub> | PPLP10% | Li battery indicates that there is a low interfacial resistance

**Fig. 6** **a** Electrochemical stability test of Li | PPL10% | Li and Li | PPLP10% | Li symmetrical battery at room temperature and the current density is 0.10 mA/cm<sup>2</sup>. **(b)** The SEM images of lithium metal surface after Li | PPL10% | Li symmetric battery running for 700 h and **(c)** Li | PPLP10% | Li symmetric battery running for 1000 h. The mechanism of inhibiting lithium dendrite growth, when using the PPL10% **(d)**, without a PE film and PPLP10% **(e)**, with a PE film as solid-state electrolytes



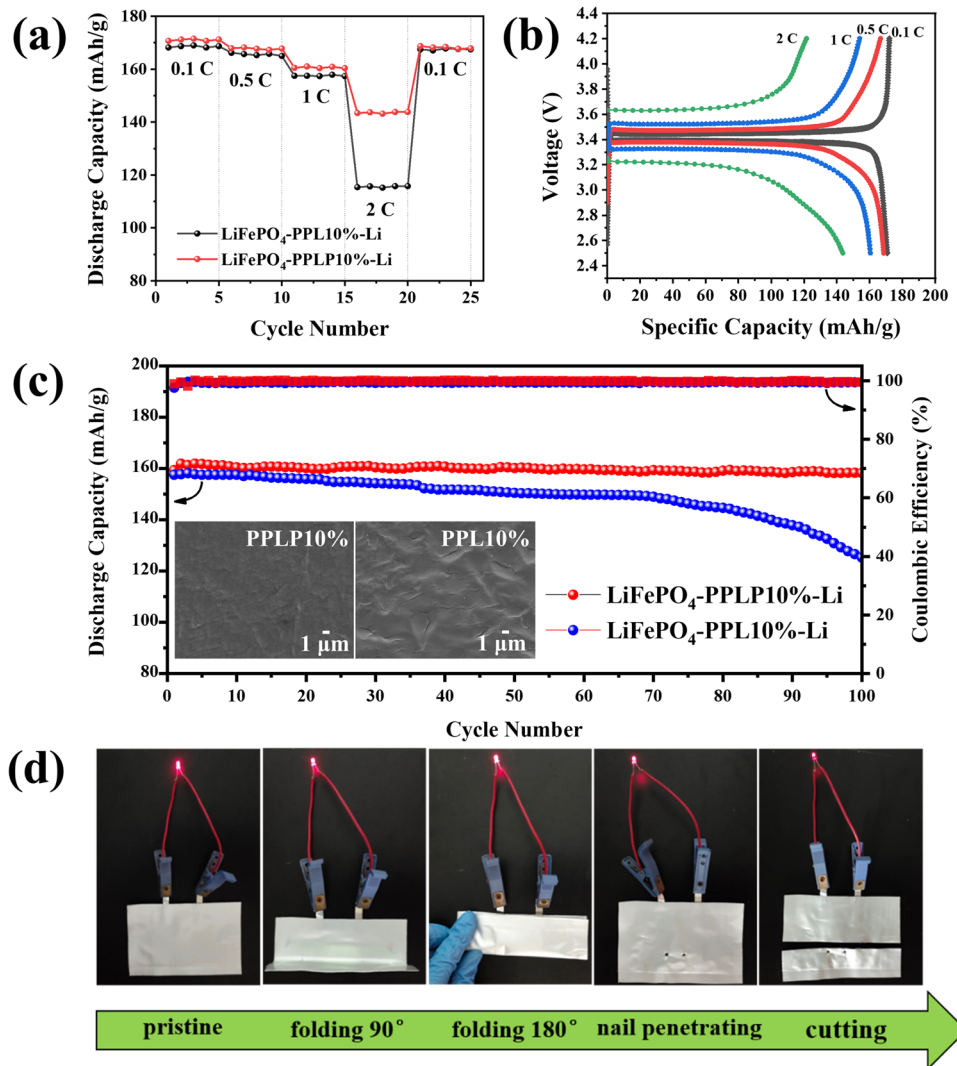
between the electrode and the PPLP10% CSE membrane, which further indicates that the sandwich-structured PPLP10% CSE membrane has excellent stability on the bilateral electrodes. Although the polarization of the battery increases and the charge-discharge specific capacity of the battery decreases when the rate reaches 2 C, the charge-discharge cycle can still go on, showing good rate performance. Figure 7c shows the constant current charge-discharge cycle results of LiFePO<sub>4</sub> | PPL10% | Li and LiFePO<sub>4</sub> | PPLP10% | Li batteries at 1 C (25 °C). It was observed that the initial discharge specific capacities of LiFePO<sub>4</sub> | PPL10% | Li and LiFePO<sub>4</sub> | PPLP10% | Li batteries were very similar, to be 159 mAh/g and 161.9 mAh/g, respectively. After 100 cycles of LiFePO<sub>4</sub> | PPL10% | Li, the specific capacity decreased

significantly, and the capacity retention was 79.5 %. However, the discharge specific capacity of LiFePO<sub>4</sub> | PPLP10% | Li battery after 100 cycles was still as high as 157.3 mAh/g, and the capacity retention was 97.8 %.

In order to further verify the inhibitory effect of sandwich-structured electrolyte on lithium dendrite, the surface morphology of lithium metal anode after 100 cycles was characterized. As illustrated in Fig. 7c (the inset photos), the surface layer of the Li metal anode in the LiFePO<sub>4</sub> | PPLP10% | Li battery is dense and smooth, but there are many dendritic cracks on the surface of the Li metal anode in the LiFePO<sub>4</sub> | PPL10% | Li battery. This indicates that the good mechanical strength of the sandwich-structured PPLP10% CSE membrane with a strong but soft PE film in



**Fig. 7** **a** Rate performance of  $\text{LiFePO}_4 \mid \text{PPL10\%} \mid \text{Li}$  and  $\text{LiFePO}_4 \mid \text{PPL10\%} \mid \text{Li}$  batteries at room temperature and 1 C rate, **b** charge and discharge voltage platform of  $\text{LiFePO}_4 \mid \text{PPL10\%} \mid \text{Li}$  and  $\text{LiFePO}_4 \mid \text{PPL10\%} \mid \text{Li}$  batteries, **c** cycle performance comparison graphs of  $\text{LiFePO}_4 \mid \text{PPL10\%} \mid \text{Li}$  and  $\text{LiFePO}_4 \mid \text{PPL10\%} \mid \text{Li}$  cells at room temperature and 1 C (the inset photos are the SEM graphs of the lithium anodes in  $\text{LiFePO}_4 \mid \text{PPL10\%} \mid \text{Li}$  and  $\text{LiFePO}_4 \mid \text{PPL10\%} \mid \text{Li}$  batteries after cycles), **d** the solid-state pouch battery runs well under a series of harsh conditions.



the middle could suppress the growing of lithium dendrites. It can be seen from Fig. S2, the discharge specific capacity of  $\text{LiFePO}_4 \mid \text{PPL10\%} \mid \text{Li}$  battery remained 150.2 mAh/g after 300 cycles at 1C (25 °C), with a capacity retention rate of 92.7%. In addition, the  $\text{Li}_4\text{Ti}_5\text{O}_{12} \mid \text{PPL10\%} \mid \text{Li}$  coin battery was assembled and tested at 1 C (25 °C) for long cycle performance. The capacity retention of  $\text{Li}_4\text{Ti}_5\text{O}_{12} \mid \text{PPL10\%} \mid \text{Li}$  was as high as 96.6% even after 500 cycles, as shown in Fig. S3. In conclusion, the cycle stability of solid-state LMBs can be improved by using a PE-containing sandwich-structured CSE. To demonstrate the practicability and safety of the sandwich-structured CSEs,  $\text{LiFePO}_4 \mid \text{PPL10\%} \mid \text{Li}$  and  $\text{LiFePO}_4 \mid \text{PPL10\%} \mid \text{Li}$  pouch batteries were assembled. As shown in Fig. S4, the  $\text{LiFePO}_4 \mid \text{PPL10\%} \mid \text{Li}$  pouch cell shows high stability with 97.5% capacity retention after 70 cycles at a rate of 0.5 C and 25 °C. In sharp contrast, the  $\text{LiFePO}_4 \mid \text{PPL10\%} \mid \text{Li}$  pouch cell undergoes significant capacity decay within 70 cycles. It can

be seen from Fig. 7d, the  $\text{LiFePO}_4 \mid \text{PPL10\%} \mid \text{Li}$  battery works well (lighting up the red LED) even under a series of harsh conditions such as be folded to 90° and 180°, nail penetration and be cut into two parts, indicating the high safety and feasibility of sandwich structured PPL10% CSEs applied to lithium metal batteries.

### Conclusions

In conclusion, a sandwich-structured PVDF-HFP / PAN-LLZTO-PE composite solid electrolyte was successfully designed and synthesized; it possessed excellent physical and electrochemical properties. The sandwich-structured PPL10% CSE showed perfect mechanical properties with tensile strength of 66.58 MPa, which was attributed to the strong support framework provided by PE film. The sandwich-structured PPL10% CSE displayed a high lithium

ion conductivity of  $2.28 \times 10^{-4}$  S/cm, wide electrochemical window of 4.8 V, and high lithium ion transference number of 0.44 at room temperature. The  $\text{LiFePO}_4$  | PPLP10% | Li battery displayed a high discharge specific capacity of 161.9 mAh/g at 1 C and a capacity retention of 92.7% after 300 cycles. Attributed to the excellent mechanical strength and electrochemical properties of the sandwich-structured PPLP10% CSE, the  $\text{LiFePO}_4$  | PPLP10% | Li pouch battery still work normally even under a series of harsh conditions. The sandwich-structured CSE described in this paper provides an ideal option for the application of high-performance solid lithium metal batteries.

**Supplementary Information** The online version contains supplementary material available at <https://doi.org/10.1007/s11581-022-04599-z>.

**Funding** This work is financially supported by the Science and Technology Commission of Shanghai Municipality (21ZR1424900, 19DZ2271100).

## Declarations

**Conflict of interest** The authors declare no competing interests.

## References

- Li M, Lu J, Chen ZW et al (2018) 30 years of lithium-ion batteries. *Adv Mater* 30:1800561
- Zhu P, Yan C, Dirican M et al (2018)  $\text{Li}_{0.33}\text{La}_{0.557}\text{TiO}_3$  ceramic nanofiber-enhanced polyethylene oxide-based composite polymer electrolytes for all-solid-state lithium batteries. *J Mater Chem A* 6:4279–4285
- Larcher D, Tarascon JM (2015) Towards greener and more sustainable batteries for electrical energy storage. *Nat Chem* 7:19–29
- Duan J, Tang X, Dai HF et al (2020) Building safe lithium-ion batteries for electric vehicles: a review. *Electrochem Energy Rev* 3:1–42
- Manthiram A, Yu XW, Wang SF (2017) Lithium battery chemistries enabled by solid-state electrolytes. *Nat Rev Mater* 2:16103
- Wei T, Zhang Z-H, Wang Z-M et al (2020) Ultrathin solid composite electrolyte based on  $\text{Li}_{6.4}\text{La}_3\text{Zr}_{1.4}\text{Ta}_{0.6}\text{O}_{12}$  / PVDF-HFP / LiTFSI / succinonitrile for high-performance solid-state lithium metal batteries. *ACS Appl Energy Mater* 3:9428–9435
- Liu L, Zhang DC, Xu XJ et al (2021) Challenges and development of composite solid electrolytes for all-solid-state lithium batteries. *Chem Res Chin Univ* 37:210–231
- Cheng X-B, Zhang R, Zhao C-Z et al (2017) Toward safe lithium metal anode in rechargeable batteries: a review. *Chem Rev* 117:10403–10473
- Wang Q, Wang HC, Wu JY et al (2021) Advanced electrolyte design for stable lithium metal anode: from liquid to solid. *Nano Energy* 80:105516
- Chen L, Qiu X, Bai Z et al (2021) Enhancing interfacial stability in solid-state lithium batteries with polymer/garnet solid electrolyte and composite cathode framework. *J Energy Chem* 52:210–217
- Chen L, Huang Y-F, Ma J et al (2020) Progress and perspective of all-solid-state lithium batteries with high performance at room temperature. *Energy Fuels* 34:13456–13472
- Xu F, Deng S, Guo Q et al (2021) Quasi-ionic liquid enabling single-phase poly(vinylidene fluoride)-based polymer electrolytes for solid-state  $\text{LiNi}_{0.6}\text{Co}_{0.2}\text{Mn}_{0.2}\text{O}_2$ /Li batteries with rigid-flexible coupling interphase. *Small Methods* 5:2100262
- Wang Z, Shen L, Deng S et al (2021) 10  $\mu\text{m}$ -thick high-strength solid polymer electrolytes with excellent interface compatibility for flexible all-solid-state lithium-metal batteries. *Adv Mater* 33:2100353
- Fan L-Z, He H, Nan C-W (2021) Tailoring inorganic–polymer composites for the mass production of solid-state batteries. *Nat Rev Mater* 6:1003–1019
- Jian Z, Hu YS, Ji X et al (2017) NASICON-Structured materials for energy storage. *Adv Mater* 29:1601925
- Zhang Q, Cao D, Ma Y et al (2019) Sulfide-based solid-state electrolytes: synthesis, stability, and potential for all-solid-state batteries. *Adv Mater* 31:e1901131
- Jiang Z, Wang S, Chen X et al (2020) Tape-casting  $\text{Li}_{0.34}\text{La}_{0.56}\text{TiO}_3$  ceramic electrolyte films permit high energy density of lithium-metal batteries. *Adv Mater* 32:e1906221
- Wang C, Fu K, Kammampata SP et al (2020) Garnet-type solid-state electrolytes: materials, interfaces, and batteries. *Chem Rev* 120:4257–4300
- Liu Q, Geng Z, Han C et al (2018) Challenges and perspectives of garnet solid electrolytes for all solid-state lithium batteries. *J Power Sources* 389:120–134
- Tan S-J, Zeng X-X, Ma Q et al (2018) Recent advancements in polymer-based composite electrolytes for rechargeable lithium batteries. *Electrochem Energy Rev* 1:113–138
- Li Z, Huang HM, Zhu JK et al (2019) Ionic conduction in composite polymer electrolytes: case of PEO: Ga-LLZO composites. *ACS Appl Mater Interfaces* 11:784–791
- Liu W, Liu N, Sun J et al (2015) Ionic conductivity enhancement of polymer electrolytes with ceramic nanowire fillers. *Nano Lett* 15:2740–2745
- Liang YF, Xia Y, Zhang SZ et al (2019) A preeminent gel blending polymer electrolyte of poly(vinylidene fluoride-hexafluoropropylene)-poly(propylene carbonate) for solid-state lithium ion batteries. *Electrochim Acta* 296:1064–1069
- Li A, Liao X, Zhang H et al (2020) Nacre-inspired composite electrolytes for load-bearing solid-state lithium-metal batteries. *Adv Mater* 32:e1905517
- Yu X, Manthiram A (2021) A review of composite polymer-ceramic electrolytes for lithium batteries. *Energy Storage Mater* 34:282–300
- Chen L, Li Y, Li S-P et al (2018) PEO/garnet composite electrolytes for solid-state lithium batteries: from “ceramic-in-polymer” to “polymer-in-ceramic”. *Nano Energy* 46:176–184
- Huo H, Chen Y, Luo J et al (2019) Rational design of hierarchical “ceramic-in-polymer” and “polymer-in-ceramic” electrolytes for dendrite-free solid-state batteries. *Adv Energy Mater* 9:1804004
- Zhang X, Liu T, Zhang S et al (2017) Synergistic coupling between  $\text{Li}_{6.75}\text{La}_3\text{Zr}_{1.75}\text{Ta}_{0.25}\text{O}_{12}$  and poly(vinylidene fluoride) induces high ionic conductivity, mechanical strength, and thermal stability of solid composite electrolytes. *J Am Chem Soc* 139:13779–13785
- Tsai C-L, Roddatis V, Chandran CV et al (2016)  $\text{Li}_7\text{La}_3\text{Zr}_2\text{O}_{12}$  interface modification for Li dendrite prevention. *ACS Appl Mater Interfaces* 8:10617–10626
- Beshahwared S L, Wu Y-S, Wu S-h, et al (2021) Flexible hybrid solid electrolyte incorporating ligament-shaped  $\text{Li}_{6.25}\text{Al}_{0.25}\text{La}_3\text{Zr}_2\text{O}_{12}$  filler for all-solid-state lithium-metal batteries. *Electrochim Acta* 366: 137348

31. Saikia D, Kumar A (2004) Ionic conduction in P(VDF-HFP)/PVDF-(PC + DEC)-LiClO<sub>4</sub> polymer gel electrolytes. *Electrochim Acta* 49:2581–2589
32. Yang H, Bright J, Chen B et al (2020) Chemical interaction and enhanced interfacial ion transport in a ceramic nanofiber-polymer composite electrolyte for all-solid-state lithium metal batteries. *J Mater Chem A* 8:7261–7272
33. Hu J, He P, Zhang B et al (2020) Porous film host-derived 3D composite polymer electrolyte for high-voltage solid state lithium batteries. *Energy Storage Mater* 26:283–289
34. Zha W, Chen F, Yang D et al (2018) High-performance Li<sub>6.4</sub>La<sub>3</sub>Zr<sub>1.4</sub>Ta<sub>0.6</sub>O<sub>12</sub> / poly(ethylene oxide) / succinonitrile composite electrolyte for solid-state lithium batteries. *J. Power Sources* 397:87–94
35. Chen RJ, Zhang YB, Liu T et al (2017) Addressing the interface issues in all-solid-state bulk-type lithium ion battery via an all-composite approach. *ACS Appl Mater Interfaces* 9:9654–9661
36. Xu SJ, Sun ZH, Sun CG et al (2020) Homogeneous and fast ion conduction of peo-based solid-state electrolyte at low temperature. *Adv Funct Mater* 30:2007172
37. Sun Y, Zhan X, Hu J et al (2019) Improving ionic conductivity with bimodal-sized Li<sub>7</sub>La<sub>3</sub>Zr<sub>2</sub>O<sub>12</sub> fillers for composite polymer electrolytes. *ACS Appl Mater Interfaces* 11:12467–12475
38. Arya A, Sharma AL (2017) Polymer electrolytes for lithium ion batteries: a critical study. *Ionics* 23:497–540

**Publisher's note** Springer Nature remains neutral with regard to jurisdictional claims in published maps and institutional affiliations.